JOURNAL OF SYNCHROTRON RADIATION
ISSN 1600-5775

Development of dispersive XAFS system for analysis of time-resolved spatial distribution of electrode reaction

Misaki Katayama,[a] Ryota Miyahara,[a] Toshiki Watanabe,[a] Hirona Yamagishi,[a] Shohei Yamashita,[a] Terue Kizaki,[b] Yoshimi Sugawara[b] and Yasuhiro Inada[a]*

[a]Department of Applied Chemistry, Ritsumeikan University, Kusatsu 525-8577, Japan, and [b]Kohzu Precision Co. Ltd, Kawasaki 215-8521, Japan. *Correspondence e-mail: yinada@fc.ritsumei.ac.jp

Received 17 March 2015
Accepted 6 July 2015

Keywords: DXAFS; imaging; polychromator; Li ion secondary battery; reaction distribution.

Supporting information: this article has supporting information at journals.iucr.org/s

Apparatus for a technique based on the dispersive optics of X-ray absorption fine structure (XAFS) has been developed at beamline BL-5 of the Synchrotron Radiation Center of Ritsumeikan University. The vertical axis of the cross section of the synchrotron light is used to disperse the X-ray energy using a cylindrical polychromator and the horizontal axis is used for the spatially resolved analysis with a pixel array detector. The vertically dispersive XAFS (VDXAFS) instrument was designed to analyze the dynamic changeover of the inhomogeneous electrode reaction of secondary batteries. The line-shaped X-ray beam is transmitted through the electrode sample, and then the dispersed transmitted X-rays are detected by a two-dimensional detector. An array of XAFS spectra in the linear footprint of the transmitted X-ray on the sample is obtained with the time resolution of the repetition frequency of the detector. Sequential measurements of the space-resolved XAFS data are possible with the VDXAFS instrument. The time and spatial resolutions of the VDXAFS instrument depend on the flux density of the available X-ray beam and the size of the light source, and they were estimated as 1 s and 100 µm, respectively. The electrode reaction of the $LiFePO_4$ lithium ion battery was analyzed during the constant current charging process and during the charging process after potential jumping.

1. Introduction

In practical electrical devices, such as secondary batteries, the spatially resolved observation of chemical reactions is important. Spatially inhomogeneous electrochemical reactions cause unexpected large current densities and accelerated aging in specific areas. X-ray absorption spectroscopy has been applied to *in situ* analyses of various chemical reactions, because the high transmittance of hard X-rays means that other material around the target sample, such as an outer shell or a solvent, can be present. Information about chemical species can be obtained even in complex systems by choosing the X-ray absorbing element. X-ray absorption fine structure (XAFS) is the best technique for *in situ* analysis of the chemical state of active materials in secondary battery systems (Leriche *et al.*, 2010). A large amount of knowledge about electrode reactions has been obtained with the synchrotron XAFS technique (Nakai *et al.*, 1997; Delmas *et al.*, 1997). Recent advancement of the XAFS technique has demonstrated the inhomogeneous reaction distribution in the electrode during the charging and discharging reaction (Katayama *et al.*, 2014; Ouvrard *et al.*, 2013). The patterns of these reaction distributions can be visualized by using the XAFS imaging technique (Katayama *et al.*, 2012). A two-dimensional

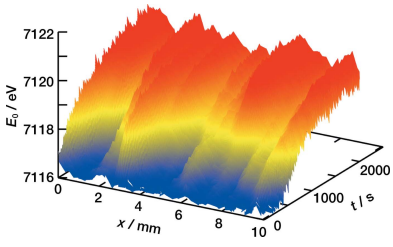

detector is used for measuring the transmitted X-ray intensity and the XAFS spectra at each position in the incident X-ray beam are spatially resolved with the element size resolution of the detector. This technique is applicable at any XAFS beamline with a non-focal X-ray beam. The inhomogeneous reaction distribution of a $LiFePO_4$ positive electrode was observed by XAFS (Katayama *et al.*, 2014; Ouvrard *et al.*, 2013) and XRD imaging techniques (Liu *et al.*, 2010). We concluded that the reaction distribution of the $LiFePO_4$ positive electrode arises from the poor electron conductivity of the active material.

The effect of the particle size of the active material on inhomogeneous chemical delithiation has been recently reported (Yoo & Kang, 2015). The particle size (less than 1 μm) may not directly affect the spatial distribution on a large scale (more than 10 μm). However, the reaction distribution on a large scale becomes an important problem for secondary batteries and thus its origin must be clarified to overcome the current limitation of the battery performance. The relationship between the reaction that occurs in a particle of the active material and the electrochemical behavior in the whole electrode is crucial for understanding the phenomena in complete batteries. One way to clarify the reaction mechanism is to analyze the reaction kinetics. The time-resolved dispersive XAFS (DXAFS) technique is very powerful for analyzing the chemical state of metal species in real time. For the DXAFS technique, a spectrum at a given energy range around the specific absorption edge can be obtained with no mechanical motions of the instrument and the technique is suitable for time-resolved measurements. The concept of the DXAFS instrument was originally published by Matsushita and Phizackerley (Matsushita & Phizackerley, 1981). The DXAFS instrument is generally composed of a bent crystal called a polychromator and a position-sensitive detector. White X-rays are irradiated to the polychromator at a given incident angle and the diffracted X-rays have different energies at each position because the incident angle to the bent crystal changes along the crystal surface. These polychromatic X-rays are focused and then dispersed. The position-sensitive detector, which is set behind the focal point, can detect X-rays with different energies at the position of each detector element. When a sample is placed at the focal point, the transmitted X-rays covered by the detector are simultaneously measured. Repeating the detector acquisition gives a sequence of XAFS spectra with the time resolution of the acquisition frequency. In principle, the measurement time for obtaining one spectrum can be shortened to the pulse width of the light source.

In this study, we have developed a measurement system that combines the time-resolved DXAFS technique with XAFS imaging. This system obtains the time-resolved reaction distribution which is useful to clarify the spatial reaction mechanism in battery electrodes. The available XAFS data as a function of both reaction time and position are very important for evaluating the origin of the inhomogeneous reaction distribution. The design of the instrument, its performance and its first application to the charging reaction of the $LiFePO_4$ positive electrode are presented in this paper.

2. Design of the vertically dispersive XAFS system

The vertically dispersive XAFS (VDXAFS) system was constructed at the DXAFS beamline BL-5 of the Synchrotron Radiation Center of Ritsumeikan University. The layout of BL-5 and a schematic of the VDXAFS instrument are shown in Fig. 1. A wide white X-ray beam is introduced to the experimental hutch through the Be windows and two slits. The VDXAFS instrument is composed of a rotating θ–2θ stage and two sets of remote stages placed on the 2θ bench to control the sample and detector positions. An adjustable counter balance is used to stabilize the movement of the 2θ rotation stage. The instrument is set in an iron experimental hutch (1650 × 1150 × 1000 mm) on the *Z*-stage table. A Pb beam stopper is used to terminate the white X-ray beam.

A 0.5 mm-thick Si(111) crystal was used as the polychromator to disperse the X-ray energy in the longitudinal plane. The distance between the light source and the polychromator crystal is 6.25 m. The thin Si crystal is held on a custom-made holder bed (Fig. 1*c*) that has a fixed concave curvature with a radius of 1 m. The curvature of the Si crystal is fixed by two presses that have a convex curvature with the same radius. The cylindrically bent Si crystal is placed on a θ rotation stage so that the pillar axis of the cylinder matches the horizontal direction of the synchrotron beam as shown in Fig. 1(*d*). The angle between the face of the Si crystal and the X-ray beam direction is set to the Bragg angle, θ, for the target X-ray energy. The dispersed X-ray beams are then diffracted in the vertical direction of 2θ *versus* the incident beam in the longitudinal plane.

The incident rectangular beam with the typical size of 4 mm (V) × 10 mm (H) becomes a linear line at the focal point, at which the sample is located by a remote sample stage. The transmitted and vertically spreading X-rays reach the two-dimensional CMOS detector (ORCA-Flash 4.0, Hamamatsu Photonics) on the 2θ bench. The vertical axis of the obtained image on the two-dimensional detector corresponds to the X-ray energy axis, whereas the horizontal axis of the image retains the spatial information in the focal line of the X-rays on the sample. Therefore, an array of XAFS spectra in the linear footprint of the X-ray on the sample is obtained with the spatial resolution of the detector element. The two-dimensional detector has 2048 × 2048 pixels and the pixel size is 6.5 μm × 6.5 μm. The Tl-doped CsI scintillator and the 1:1 optical lens system are placed in front of the two-dimensional detector. The detectable area on the scintillator is 13 mm × 13 mm.

3. Energy uniformity of the polychromator

The XAFS spectra of the standard metal foils were measured by using the VDXAFS instrument, and are compared with those measured at the conventional XAFS beamline in Figs. 2(*a*) and 2(*b*). The reference spectra were obtained by using a Si(220) double-crystal monochromator at BL-3 of the Synchrotron Radiation Center. The spectra measured by the VDXAFS instrument were collected with an exposure time of

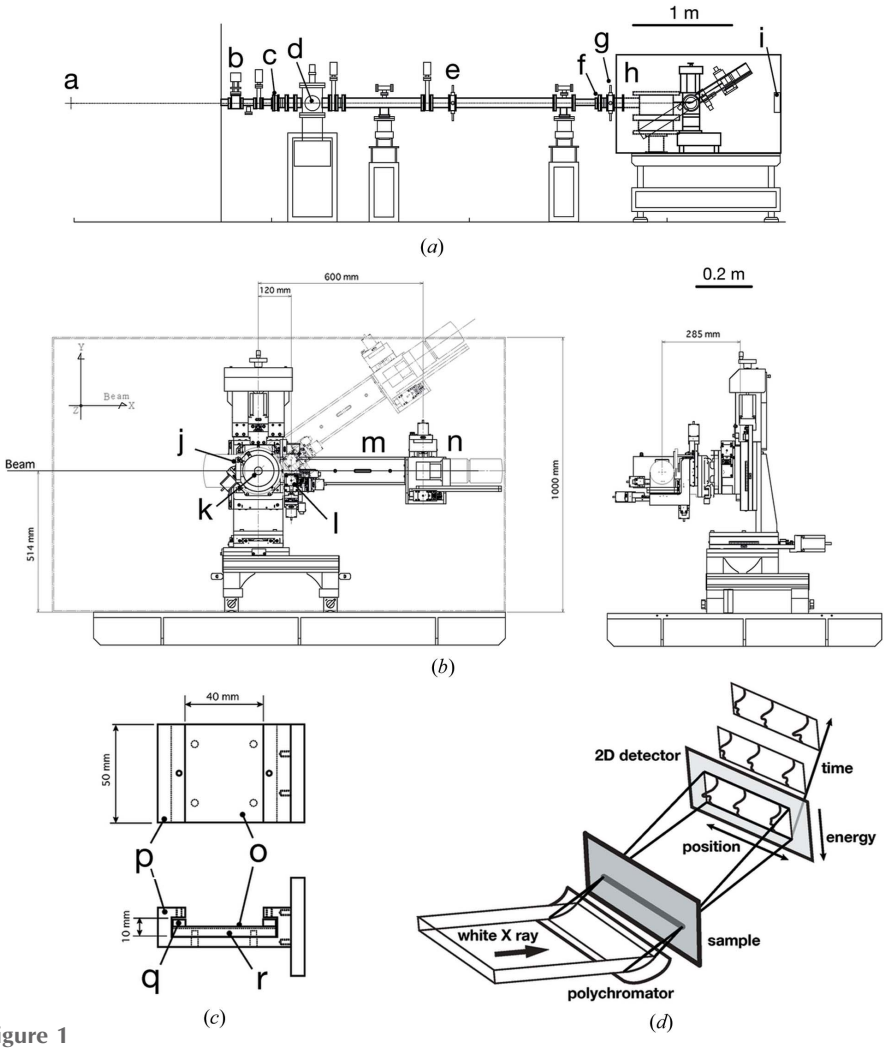

Figure 1
Side view of the DXAFS beamline BL-5 (*a*) and the VDXAFS instrument (*b*). Legend: a, light source; b, beam shutter; c, mask; d, Be window; e, first slit; f, Be window; g, second slit; h, experimental hutch; i, direct beam stopper; j, θ–2θ goniometer; k, polychromator chamber; l, sample stage; m, 2θ bench; n, two-dimensional detector. (*c*) Sketch of polychromator holder. Legend: o, bent Si crystal; p, holder jacket; q, fixed-curvature presses; r, crystal bed. (*d*) Optical arrangement of polychromator, sample and two-dimensional detector.

5 s and the curves for different accumulated width are shown in the figure. The statistics of the observed spectra are satisfactory for XAFS analysis and thus the time resolution of the VDXAFS instrument is estimated to be about 1 s. Because the time resolution strongly depends on the available X-ray flux, the value is for the VDXAFS instrument used at the Synchrotron Radiation Center of the Ritsumeikan University. The energy resolution of the cylindrically curved Si(111) crystal is also sufficient to analyze the XANES spectrum. The available energy range depends on the Bragg angle of the polychromator, because it is determined by the width of the footprint on the crystal surface. The accessible energy range was about 500 eV at the Co *K*-edge and 700 eV at the Cu *K*-edge.

The uniformity of the energy axis in the horizontal direction was confirmed by measuring several absorption edges. Fig. 2(*c*) shows the detector pixel at the Co *K*-, Eu L_{II}- and Eu L_{I}-edges. These edges were simultaneously measured in one measurement of the VDXAFS spectra. The flat shape of the plot for each edge means that the same energy axis is used for each horizontal position. This confirmed that the developed bent crystal has the desired cylindrical shape with no horizontal distortion.

4. Spatial resolution

The distance between the crystal center and the focal point, q, is given by

$$q = (Rp\sin\theta)/(2p - R\sin\theta), \qquad (1)$$

where R is the bending radius of the polychromator, p is the distance between the light source and the crystal center, and θ is the incident angle of the X-rays to the polychromator at the beam center. The q values calculated by equation (1) are 0.14, 0.13 and 0.11 m for the *K*-edge of Fe, Co and Cu, respectively, and these distances were in agreement with the experimental values. The focused beam has a linear shape and the focus size of the polychromatic X-rays is used to decide on the observation area of the sample. The observed image of the focused beam is given in Fig. 3(*a*). The vertical intensity profile in Fig. 3(*b*) is asymmetrical because of the optical aberration of the cylindrical polychromator. When the vertical size of the incident white X-ray beam was set to 4 mm, the focus size was estimated to be 70 µm at the Fe *K*-edge as the FWHM of the intensity profile peak. The focus size can be decreased by decreasing the vertical size of the incident X-rays, although this reduces the accessible energy range.

The beam divergence in the horizontal direction was estimated by using a knife-edge. Fig. 3(*c*) shows the horizontal intensity profile measured by changing the detector position, when the knife-edge was placed at the focal point. The decrease in the edge tailing is explained by considering the size of the light source [1.3 mm (H) × 0.14 mm (V) at the Synchrotron Radiation Center] and the ratio of the distance from the light source and the separation between the focus point and the detector. The profile suggests a horizontal spatial resolution of about 100 µm. This resolution is related to the size of the light source and is greatly improved by using the VDXAFS instrument at another synchrotron radiation facility with a much smaller light source. From the vertical focus size of 70 µm and the horizontal divergence of 100 µm, the spatial resolution of the VDXAFS instrument is estimated to be about 100 µm (H) × 100 µm (V). This speciation is inferior

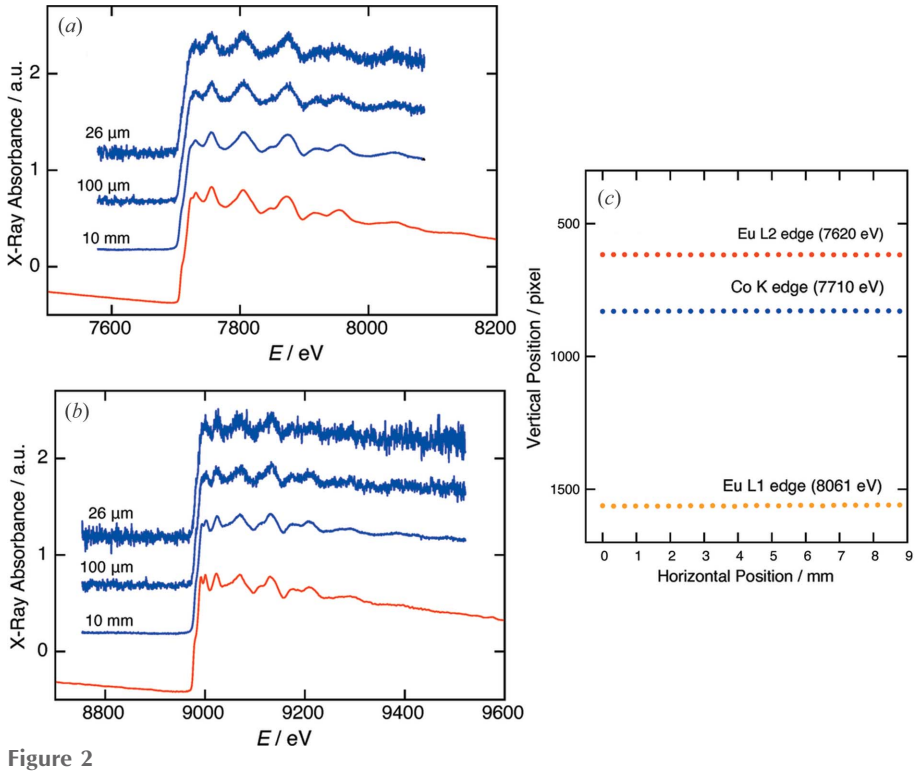

Figure 2
XANES spectra observed by using the Si(111) bent crystal polychromator (blue) and the Si(220) double-crystal monochromator (red) for (*a*) Co foil at the Co *K*-edge and (*b*) Cu foil at the Cu *K*-edge. Accumulated widths are shown in the figure. Absorption-edge positions of the Co *K*-, Eu L_{II}- and L_{I}-edges measured at a fixed optical configuration are shown in (*c*).

to current advanced nanobeam techniques, although our VDXAFS instrument can make simultaneous XAFS measurements and their time-resolved acquisition at points linearly aligned in the range of several centimeters. This is powerful for analyzing the spatial correlation of the chemical state changeover.

5. Time- and space-resolved XAFS spectra of an electrode sample

We used the VDXAFS instrument to analyze the dynamic change of the reaction distribution in the $LiFePO_4$ positive electrode of a lithium ion secondary battery, in which the inhomogeneous progress of the electrode reaction has been reported for both the charging and discharging processes (Katayama *et al.*, 2014; Ouvrard *et al.*, 2013). The $LiFePO_4$ and Li electrodes separated by polypropylene sealed in an Al-laminated bag were prepared by a previously reported procedure (Katayama *et al.*, 2014). The charging process was performed at a constant current (1C) condition to observe the heterogeneous reaction distribution of $LiFePO_4$ using the developed VDXAFS instrument.

The observed XANES spectra at the Fe *K*-edge during the charging process under a constant current of 1C are shown in Fig. 4. The XANES spectra at 27 different positions on the $LiFePO_4$ electrode are given at six charging times. One spectrum was obtained by using data from an area of 300 μm (H) × 100 μm (V) for a 5 s acquisition time. Initially, all spectra show the white line peak top at the same X-ray energy, and it moves to a higher energy inhomogeneously. The shift of the absorption-edge energy of *ca* 4 eV agreed with the difference in those of $LiFePO_4$ and $FePO_4$ measured by the conventional XAFS instrument. The oxidation of Fe in area **A** proceeds before that in area **B** (Fig. 4), clearly indicating that an inhomogeneous reaction distribution appears in the observed area. The spatial scale of the reaction distribution is equivalent to that observed in the two-dimensional XAFS imaging map shown in Fig. S1 (supporting information). The expansion of the reacting spot according to the depth of charge agrees with that observed by the *in situ* two-dimensional XAFS imaging technique (Katayama *et al.*, 2014). We have concluded that the reaction distribution is caused by the difference in the electric conductivity because the reaction distribution shows reproducibility at the successive cycles and reversibility between the charging and discharging processes.

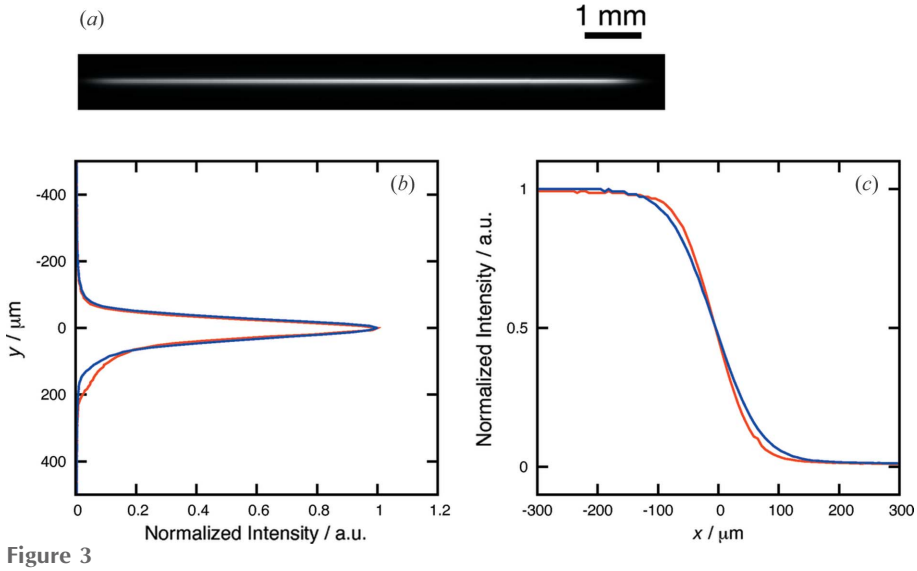

Figure 3
(*a*) Focused beam shape, (*b*) vertical profile of the X-ray intensity at the energies for Fe *K* (blue) and Co *K* (red) and (*c*) the horizontal profile of the X-ray intensity after a knife-edge measured at the focal point. The detector was placed 290 (red) and 390 (blue) mm away from the focal point.

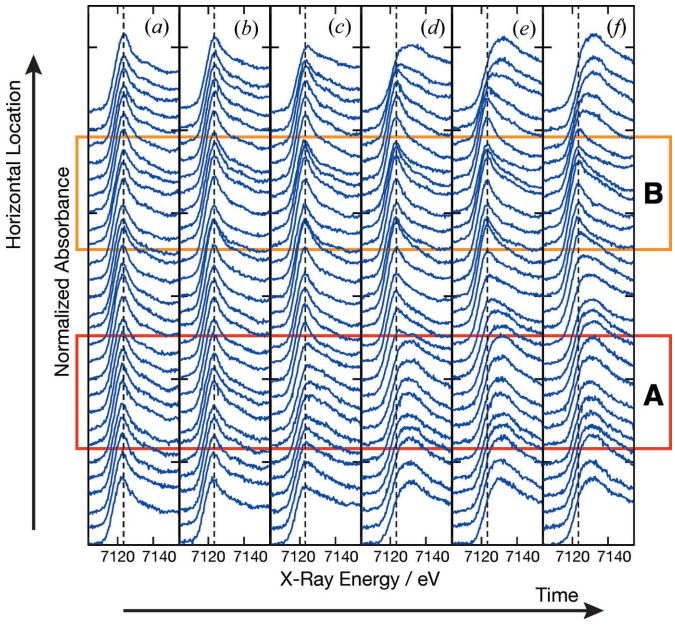

Figure 4
Fe *K*-edge XANES spectra of the $LiFePO_4$ electrode during a constant current charging process at 0 (*a*), 440 (*b*), 1020 (*c*), 1590 (*d*), 2170 (*e*) and 2750 s (*f*) after the start of charging.

The similarity of such heterogeneity suggests that the observed distribution was caused by the spatially different electric conductance generated by the inhomogeneous carbon network in the $LiFePO_4$ cathode sheet.

We have further measured the charging process after a rapid potential jump to 4.2 V using the developed VDXAFS instrument. The rapid potential jump is used to decide the initiation time to start the charging process and the chemical state change of the Fe species was measured during the constant voltage charging process without any limitations of the total current. Fig. S2 shows the total current of the battery and the averaged energy of the Fe *K*-edge in the observed area during the constant voltage charging process after the potential jump. The changeover of the chemical state of Fe in the measured area is almost consistent with the integrated current for the whole electrode. Fig. 5 shows the sequence of the one-dimensional chemical map during the constant voltage charging process after the potential jump. The three-dimensional plot obtained of the chemical state of Fe as a function of time and location clearly shows that the electrode reactions at $x \approx 1$ and 4 mm are delayed compared with those at $x \approx 0$, 2 and 9 mm. The inhomogeneous progress that resembles mountain ridges suggests that the Fe oxidation, *i.e.* the delithiation, progresses radially at some reaction channels. The result for the rapid potential jump experiment shows that the time-course change of the Fe chemical state at each position differs from the time-course change of the electrode current. The detailed analysis of the time-course curve of the chemical state as a function of both the reaction time and position will provide useful insights to understand the chemical reactions in the composite electrode of the batteries.

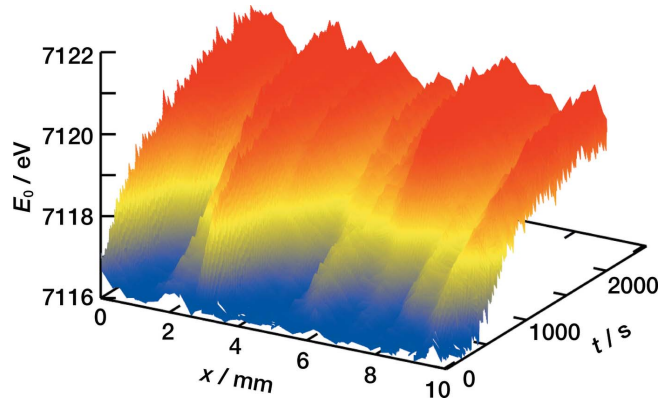

Figure 5
Three-dimensional plot of VDXAFS data for a 4.2 V charging process of the $LiFePO_4$ battery. Change over time of the one-dimensional chemical state map for the Fe species.

6. Conclusion

We have developed a VDXAFS instrument for simultaneous time- and space-resolved XAFS measurements to analyze the inhomogeneous reaction distribution in the positive electrode of lithium ion secondary batteries. We confirmed that the cylindrically bent polychromator has sufficient energy resolution and horizontal uniformity to analyze the XAFS spectra. The VDXAFS instrument makes simultaneous XAFS measurements possible and their time-resolved acquisition at points linearly aligned in the range of several centimeters. The practical time and space resolution were 1 s and 100 µm (H) × 100 µm (V), respectively, at the Synchrotron Radiation Center of Ritsumeikan University. The instrument successfully obtained the sequence of the one-dimensional chemical map for the Fe species during a constant voltage charging process after the potential jump for the $LiFePO_4$ electrode reaction. The reaction channels and radial propagation around them, which has been observed previously by using two-dimensional XAFS imaging, were reproduced in the present study.

Acknowledgements

This work was partially supported by the Research and Development Initiative for Scientific Innovation of New Generation Battery (RISING) project from the New Energy and Industrial Technology Development Organization (NEDO), Japan. Some of the VDXAFS measurements were carried out under the approval of PF program advisory committee (Nos. 2012G020 and 2014G542).

References

Delmas, C., Pérès, J. P., Rougier, A., Demourgues, A., Weill, F., Chadwick, A., Broussely, M., Perton, F., Biensan, Ph. & Willmann, P. (1997). *J. Power Sources*, **68**, 120–125.
Katayama, M., Sumiwaka, K., Hayashi, K., Ozutsumi, K., Ohta, T. & Inada, Y. (2012). *J. Synchrotron Rad.* **19**, 717–721.
Katayama, M., Sumiwaka, K., Miyahara, R., Yamashige, H., Arai, H., Uchimoto, Y., Ohta, T., Inada, Y. & Ogumi, Z. (2014). *J. Power Sources*, **269**, 994–999.

Leriche, J. B., Hamelet, S., Shu, J., Morcrette, M., Masquelier, C., Ouvrard, G., Zerrouki, M., Soudan, P., Belin, S., Elkaïm, E. & Baudelet, F. (2010). *J. Electrochem. Soc.* **157**, A606–A610.
Liu, J., Kunz, M., Chen, K., Tamura, N. & Richardson, T. J. (2010). *J. Phys. Chem. Lett.* **1**, 2120–2123.
Matsushita, T. & Phizackerley, R. P. (1981). *Jpn. J. Appl. Phys.* **20**, 2223–2228.
Nakai, I., Takahashi, K., Shiraishi, Y., Nakagome, T., Izumi, F., Ishii, Y., Nishikawa, F. & Konishi, T. (1997). *J. Power Sources*, **68**, 536–539.
Ouvrard, G., Zerrouki, M., Soudan, P., Lestriez, B., Masquelier, C., Morcrette, M., Hamelet, S., Belin, S., Flank, A. M. & Baudelet, F. (2013). *J. Power Sources*, **229**, 16–21.
Yoo, S. & Kang, B. (2015). *Electrochim. Acta*, **151**, 270–275.